Modeling and Analysis of Series-None Compensation for Wireless Power Transfer Systems With a Strong Coupling

Yiming Zhang, *Member, IEEE*, Tianze Kan, *Student Member, IEEE*, Zhengchao Yan, *Student Member, IEEE*, Yunhe Mao, Zhixian Wu, and Chunting Chris Mi, *Fellow, IEEE*

***Abstract*—In some applications of wireless power transfer, such as wireless charging of consumer electronics and electric buses, the coupling between the transmitter and the receiver is strong in order to improve efficiency. With a strong coupling, the compensation on the receiver side can be eliminated to achieve a high-level integration of the receiver device and a smaller receiver-side loss, forming a series-none (SN) topology, which has not been fully investigated before. The commonly used first harmonic approximation method for the SN topology has discrepancies with a low-power output and cannot fully reveal the characteristics of the SN topology. Therefore, this paper establishes a model of the SN topology and derives the analytical expressions of the transmitter and receiver currents based on differential equations. The distortion of the receiver current is studied. The coil-to-coil efficiency is obtained and its maximum condition is investigated. The SN topology offers approximately the same efficiency as the SS topology when the coupling is strong and the coil quality factors are large. Theoretical calculations and experimental results confirm the analysis.**

***Index Terms*—Compact and small size, differential equations, LLC converter, series-none (SN) compensation, wireless charging, wireless power transfer (WPT).**

I. Introduction

THERE have been great advancements of Wireless Power Transfer (WPT) technology [1]–[4] that can be applied where the conventional wired power transfer is inconvenient, expensive, hazardous, or even impossible, such as electric vehicles (EVs), consumer electronics, implantable medical devices, and special industrial charging applications like mining and underwater devices. Inductive power transfer (IPT), or magnetic induction WPT, is the most widely applied WPT technology that employs the magnetic field for power transfer. In IPT, compensations are generally required to increase efficiency and decrease the VA rating of the inverter. Typical compensations include series (S) compensation [5], [6], parallel (P) compensation [7], [8], and LCC compensation [9], [10]. The topologies of SS, PP, and LCC-LCC are shown in Fig. 1.

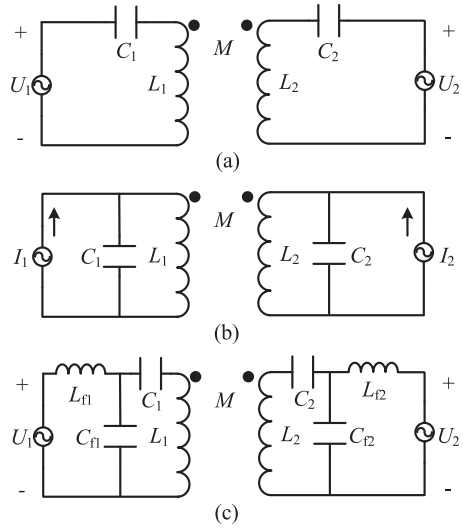

Fig. 1. Topologies of a WPT system. (a) SS. (b) PP. (c) LCC–LCC.

In some charging scenarios, a strong coupling is required to achieve high efficiency. Typical examples are high-power wireless charging for EVs [11], where the gap between the transmitter and the receiver is much smaller than the coil diameter, and wireless charging for consumer electronics [12]. To facilitate the integration of the receiver into the EV or the consumer electronics, a compact receiver is required. With a strong coupling, the receiver compensation can be eliminated to reduce the size, weight, and cost of the receiver while still maintaining a high efficiency. Because a full-bridge voltage-source inverter (VSI) is adopted as the source for the WPT system, an S compensation is selected on the primary side, which can be directly connected to the VSI. With an S compensation for the transmitter, a series-none (SN) compensation for a WPT system with a strong coupling is formed. The SN compensation can be applied where a compact and low-cost receiver of a WPT system is required. The coupling between the transmitter and the receiver should be strong and the coil quality factors should be large

Manuscript received January 10, 2018; revised March 22, 2018; accepted May 3, 2018. Date of publication May 9, 2018; date of current version December 7, 2018. This work is supported by Huawei Technologies Co., Ltd under Grant 9406139. Recommended for publication by Associate Editor C. K. Tse. *(Corresponding author: Chris Mi.)*

Y. Zhang, T. Kan and C. C. Mi are with the Department of Electrical and Computer Engineering, San Diego State University, San Diego, CA 92182 USA (e-mail: zhangym07@gmail.com; bigtreehust@gmail.com; mi@ieee.org).

Z. Yan is with the School of Marine Science and Technology, Northwestern Polytechnical University, Xi'an 710072, China, and also with the Department of Electrical and Computer Engineering, San Diego State University, San Diego, CA 92182 USA (e-mail: yanzc1991@gmail.com).

Y. Mao and Z. Wu are with the Huawei Technologies Co., Ltd., Shenzhen 518000, China (e-mail: maoyunhe@huawei.com; wuzhixian3@huawei.com).

Color versions of one or more of the figures in this paper are available online at http://ieeexplore.ieee.org.

Digital Object Identifier 10.1109/TPEL.2018.2835307

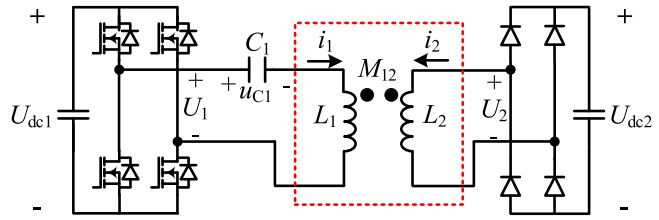

Fig. 2. WPT system with an SN compensation.

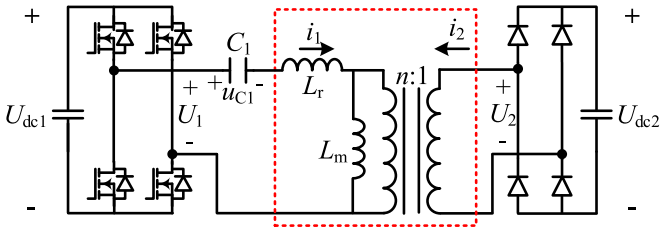

Fig. 3. All-primary-referred model of a WPT system with an SN compensation.

to achieve high efficiency. In [13], [14], a similar SN topology was employed, but the analysis was based on first harmonic approximation (FHA), which is not accurate enough.

In this paper, a strongly coupled WPT system with an SN compensation is studied and compared with the LLC converter. The models of the SN topology at the resonant frequency are established based on both FHA and the differential equations (DE). Analytical expressions of the transmitter and receiver currents are derived. The coil-to-coil efficiency is analyzed and maximized. Theoretical calculations and experimental verifications are conducted to confirm the analysis.

II. Comparison Between SN Topology and LLC Converter

The topology of a WPT system with an SN compensation is depicted in Fig. 2, where $U_{\rm dc1}$ and U_1 are the input dc voltage and the output ac voltage of the inverter, respectively; i_1 and L_1 are the current and self-inductance of the transmitter, respectively; $U_{\rm dc2}, U_2, i_2,$ and L_2 are their counterparts on the receiver side; M_{12} is the mutual inductance between the transmitter and the receiver; C_1 is the capacitance of the transmitter; and u_{C1} is the capacitor voltage.

The model in Fig. 3 resembles the LLC converter [15]. L_r can be obtained as the primary inductance in Fig. 2 when the secondary is short-circuited. L_m is the difference between L_1 and L_r. L_r, L_m, and n can be expressed, respectively, by

$$L_r = \frac{1}{j\omega}\left(j\omega L_1 + \frac{(\omega M_{12})^2}{j\omega L_2}\right) = L_1 - \frac{M_{12}^2}{L_2} = \left(1 - k_{12}^2\right) L_1 \tag{1}$$

$$L_m = L_1 - L_r = \frac{M_{12}^2}{L_2} = k_{12}^2 L_1 \tag{2}$$

$$n = \frac{M_{12}}{L_2} = k_{12}\sqrt{\frac{L_1}{L_2}} \tag{3}$$

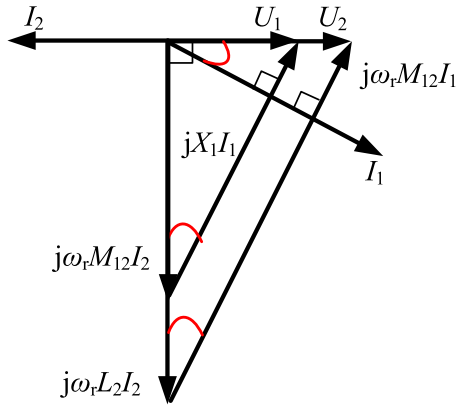

Fig. 4. Phasor diagram of transmitter and receiver voltages and currents.

where k_{12} is the coupling coefficient of the transmitter and the receiver, defined as

$$k_{12} = \frac{M_{12}}{\sqrt{L_1 L_2}}. \tag{4}$$

The angular resonant frequency of L_r and C_1 can be calculated by

$$\omega_r = \frac{1}{\sqrt{L_r C_1}}. \tag{5}$$

At ω_r, U_1, and U_2 are in phase. $U_{\rm dc1}$ and $U_{\rm dc2}$ are positively or negatively connected to the resonant circuit simultaneously. Ideally, the relationships between U_1 and U_2, and also $U_{\rm dc1}$ and $U_{\rm dc2}$ are

$$\frac{U_1}{U_2} = \frac{U_{\rm dc1}}{U_{\rm dc2}} = n. \tag{6}$$

III. Modeling and Analysis

A. Model Based on FHA

Based on FHA, U_1 and U_2 in Fig. 2 can be expressed by

$$\begin{cases} U_1 = \dfrac{2\sqrt{2}}{\pi} U_{\rm dc1} \\ U_2 = \dfrac{2\sqrt{2}}{\pi} U_{\rm dc2}. \end{cases} \tag{7}$$

U_1 and U_2 satisfy (6). Since it is a voltage-source converter, the receiver current I_2 is determined by the load. The transmitter reactance X_1 is defined by

$$X_1 = \omega_r L_1 - \frac{1}{\omega_r C_1}. \tag{8}$$

Assume that the rectifier is resistive and the system is operated at the resonant angular frequency ω_r. Based on the directions defined in Fig. 2, the phasor diagram of the transmitter and receiver voltages and currents is depicted in Fig. 4. For a given U_1 and I_2, U_2 and I_1 can be calculated by

$$U_2 = \frac{L_2}{M_{12}} U_1 = \frac{U_1}{n} \tag{9}$$

$$I_1 = \frac{\sqrt{U_2^2 + (\omega_r L_2 I_2)^2}}{\omega_r M_{12}} = \frac{1}{n}\sqrt{\frac{U_1^2}{(\omega_r M_{12})^2} + I_2^2}. \quad (10)$$

The phase difference between U_1 and I_1, which is the phase angle of the input impedance, can be calculated by

$$\beta = \arctan\frac{U_2}{\omega_r L_2 I_2} = \arctan\frac{R_{Lac}}{\omega_r L_2} \quad (11)$$

where R_{Lac} is the equivalent ac load resistance.

We can see from Fig. 4 that the input impedance of the WPT system with an SN compensation is always inductive, which is good for achieving zero voltage switching (ZVS).

The output power can be calculated by

$$P_{\text{out}} = U_2 I_2 = \frac{U_2^2}{\omega_r L_2}\cot\beta = \frac{8}{\pi^2}\frac{U_{\text{dc2}}^2}{\omega_r L_2}\cot\beta. \quad (12)$$

B. Model Based on DE

FHA may not always be true with the SN topology, especially when the currents are not sinusoidal. To describe the SN topology, u_{C1}, i_1, and i_2 are chosen as the state variables and the DE concerning these three variables are developed below. For the first half cycle, when U_{dc1} and U_{dc2} are positively connected to the resonant circuit, the model in Fig. 2 can be built by

$$\begin{cases} U_{\text{dc1}} = u_{C1} + L_1\dfrac{di_1}{dt} + M_{12}\dfrac{di_2}{dt} \\ U_{\text{dc2}} = L_2\dfrac{di_2}{dt} + M_{12}\dfrac{di_1}{dt} \\ i_1 = C_1\dfrac{du_{C1}}{dt}. \end{cases} \quad (13)$$

The initial conditions to constrain (13) are

$$\begin{cases} i_1(0) = -i_1(\pi) \\ i_2(0) = -i_2(\pi) \\ u_{C1}(0) = -u_{C1}(\pi) \\ i_2(0) = 0. \end{cases} \quad (14)$$

For the second half cycle, the DE and the initial conditions are shown, respectively, in the following equations:

$$\begin{cases} -U_{\text{dc1}} = u_{C1} + L_1\dfrac{di_1}{dt} + M_{12}\dfrac{di_2}{dt} \\ -U_{\text{dc2}} = L_2\dfrac{di_2}{dt} + M_{12}\dfrac{di_1}{dt} \\ i_1 = C_1\dfrac{du_{C1}}{dt} \end{cases} \quad (15)$$

$$\begin{cases} i_1(\pi) = -i_1(2\pi) \\ i_2(\pi) = -i_2(2\pi) \\ u_{C1}(\pi) = -u_{C1}(2\pi) \\ i_2(\pi) = 0. \end{cases} \quad (16)$$

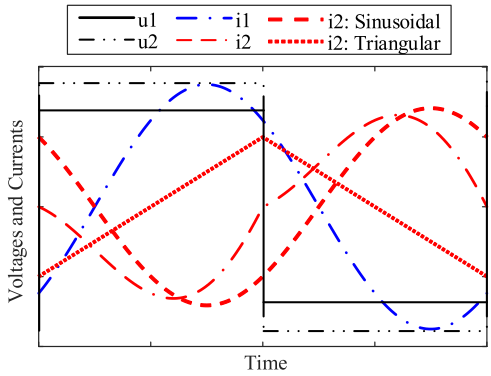

Fig. 5. Primary and secondary voltage and current waveforms.

Based on (13)–(16), the analytical expressions of the transmitter and receiver currents can be derived as

$$\begin{cases} i_1 = \dfrac{\pi U_{\text{dc2}}}{2\omega_r M_{12}}\dfrac{\sin(\omega_r t - \beta)}{\sin\beta} \\ i_2 = -\dfrac{\pi U_{\text{dc2}}}{2\omega_r L_2} \\ \quad \left\{ \dfrac{\sin(\omega_r t - \beta)}{\sin\beta} \right. \\ \quad \left. \underline{+(-1)^{\text{floor}\left(\frac{\omega_r t}{\pi}\right)}\left[\dfrac{2\omega_r t}{\pi} - 2\text{floor}\left(\dfrac{\omega_r t}{\pi}\right) - 1\right]} \right\} \end{cases} \quad (17)$$

where floor (B) represents the function that rounds the element of B toward the next smaller integer. β is the phase difference between u_1 and i_1 and $0 < \beta < \pi/2$. It can be found that the transmitter current is purely sinusoidal, while the receiver current has two components: the sinusoidal component and the triangular component (the underlined term in (17)). When β is 45°, the waveforms of the transmitter and receiver voltages and currents, together with the two components of the receiver current, are shown in Fig. 5. The distorted receiver current is caused by the composition of the sinusoidal and triangular components. The triangular component of the receiver current does not contribute to the power transfer but makes the receiver current distorted. The sinusoidal component, which contributes to the power transfer, is not 180° out of phase with the receiver voltage u_2. Instead, there is a phase difference between the receiver voltage and the receiver current. The amplitude of the receiver current is smaller than the sinusoidal component due to the existence of the triangular component. Also, the receiver current is half-wave symmetrical. FHA is not accurate in this case, especially when the receiver current is small.

According to (17), the sinusoidal component of the receiver current is in reverse proportion to the phase difference between the transmitter voltage and current β, while the triangular component is independent of β. The smaller the β, the larger the transmitter and receiver currents. Therefore, when the phase difference is small enough, the impact of the triangular component can be ignored.

At time 0, the transmitter current can be expressed by

$$i_1(0) = -\frac{\pi U_{\mathrm{dc2}}}{2\omega_r M_{12}} \tag{18}$$

which is always negative, indicating that the WPT system with an SN compensation can achieve ZVS for higher inverter efficiency.

The root-mean-square (RMS) values of i_1 and i_2 are

$$\begin{cases} I_1 = \dfrac{\pi U_{\mathrm{dc2}}}{2\sqrt{2}\omega_r M_{12}\sin\beta} \\ I_2 = \dfrac{\pi U_{\mathrm{dc2}}}{2\omega_r L_2}\sqrt{\dfrac{1}{2\sin^2\beta} + \dfrac{1}{3} - \dfrac{8}{\pi^2}}. \end{cases} \tag{19}$$

One of the advantages of the SN topology is that it achieves a compact receiver structure with reduced cost, weight, volume, and loss. For an identical transmission coil system, where $L_1 = L_2$, the ratio of the RMS values of the transmitter current and the receiver current can be obtained from (19) as

$$\frac{I_1}{I_2} = \frac{1}{k_{12}\sqrt{1 + \left(\frac{1}{3} - \frac{8}{\pi^2}\right)2\sin^2\beta}}. \tag{20}$$

This ratio is always larger than 1 and the larger the phase difference β, the larger this ratio. Due to the fact that there is a matching capacitance on the transmitter side, while there is none on the receiver side, the equivalent resistance of the transmitter R_1 is larger than that of the receiver R_2. Therefore, the loss on the receiver side is smaller than that on the transmitter side, which is good for the thermal design of the receiver.

The dc current of the rectifier can be calculated as

$$\begin{aligned} I_{\mathrm{dc2}} &= \left| \frac{\omega_r}{\pi}\int_0^{\pi/\omega_r} \frac{\pi U_{\mathrm{dc2}}}{2\omega_r L_2}\left[-\frac{\sin(\omega_r t - \beta)}{\sin\beta} - 1 + \frac{2\omega_r t}{\pi}\right] dt \right| \\ &= \frac{U_{\mathrm{dc2}}}{\omega_r L_2}\cot\beta. \end{aligned} \tag{21}$$

The output power and the input power can be calculated as

$$P_{\mathrm{out}} = U_{\mathrm{dc2}} I_{\mathrm{dc2}} = \frac{U_{\mathrm{dc2}}^2}{\omega_r L_2}\cot\beta \tag{22}$$

$$P_{\mathrm{in}} = U_1 I_1 \cos\beta = \frac{U_{\mathrm{dc1}} U_{\mathrm{dc2}}}{\omega_r M_{12}}\cot\beta. \tag{23}$$

Since the coil loss is not considered in the derivation, letting $P_{\mathrm{out}} = P_{\mathrm{in}}$ yields

$$\begin{cases} U_{\mathrm{dc2}} = \dfrac{L_2}{M_{12}} U_{\mathrm{dc1}} = \dfrac{U_{\mathrm{dc1}}}{n} \\ I_{\mathrm{dc2}} = \dfrac{M_{12}}{L_2} I_{\mathrm{dc1}} = n I_{\mathrm{dc1}}. \end{cases} \tag{24}$$

This is the characteristic shown in the LLC converter that there is a certain ratio of the output voltage and the input voltage. In addition, the smaller the β is, the larger the output power will be.

From (21), we have

$$\beta = \arctan\frac{U_{\mathrm{dc2}}}{\omega_r L_2 I_{\mathrm{dc2}}} = \arctan\frac{R_{L\mathrm{dc}}}{\omega_r L_2} \tag{25}$$

where $R_{L\mathrm{dc}}$ is the equivalent dc load resistance.

Comparing (11) and (25), we can know that the calculated phase difference based on FHA is smaller than that based on DE, because $R_{L\mathrm{ac}} > R_{L\mathrm{dc}}$. Thus, the calculated transmitter current based on FHA would be smaller than the results from DE, which are closer to the actual values. The amplitude of the transmitter current affects the selection of the power switches of the inverter and the resonant capacitors. Therefore, it is more precise to analyze the WPT system with an SN compensation based on DE.

The coil-to-coil efficiency can be calculated as

$$\begin{aligned} \eta_{\mathrm{coil}} &= \frac{P_{\mathrm{out}}}{P_{\mathrm{out}} + I_1^2 R_1 + I_2^2 R_2} \\ &= \frac{1}{1 + \frac{\pi^2}{4}\left(\frac{1}{k_{12}^2 Q_1} + \frac{1}{Q_2}\right)\frac{1}{\sin 2\beta} + \frac{\pi^2}{4Q_2}\left(\frac{1}{3} - \frac{8}{\pi^2}\right)\tan\beta} \end{aligned} \tag{26}$$

where Q_1 and Q_2 are the quality factors of the transmitter and the receiver, respectively. They are defined as

$$Q_1 = \frac{\omega_r L_1}{R_1}, Q_2 = \frac{\omega_r L_2}{R_2}. \tag{27}$$

Note that $0 < \beta < \pi/2$. By taking $\partial\eta_{\mathrm{coil}}/\partial\beta = 0$, the optimal β can be obtained. Assuming that $Q_1 = Q_2 = Q$, the optimal β can be derived as

$$\beta_{\mathrm{opt}} = \arctan\sqrt{\frac{\frac{1}{k_{12}^2} + 1}{\frac{1}{k_{12}^2} + 1 + 2\left(\frac{1}{3} - \frac{8}{\pi^2}\right)}} \approx \frac{\pi}{4}. \tag{28}$$

The maximum coil-to-coil efficiency can be calculated as

$$\eta_{\mathrm{coil\text{-}max\text{-}SN}} = \frac{1}{1 + \frac{\pi^2}{4}\frac{1}{Q}\left(\frac{1}{k_{12}^2} + 1 + \frac{1}{3} - \frac{8}{\pi^2}\right)}. \tag{29}$$

Thus, conclusions can be drawn that the coil-to-coil efficiency of the SN topology peaks at the phase difference of $\pi/4$. The corresponding dc current of the rectifier and the output power are calculated as

$$I_{\mathrm{dc2\text{-}opt}} = \frac{U_{\mathrm{dc2}}}{\omega_r L_2} \tag{30}$$

$$P_{\mathrm{out\text{-}opt}} = \frac{U_{\mathrm{dc2}}^2}{\omega_r L_2}. \tag{31}$$

According to [16], the maximum coil-to-coil efficiency of the SS topology can be simplified as

$$\eta_{\mathrm{coil\text{-}max\text{-}SS}} = \left(\frac{k_{12}Q}{1 + \sqrt{1 + (k_{12}Q)^2}}\right)^2 \approx \frac{k_{12}Q}{k_{12}Q + 2}. \tag{32}$$

The maximum coil-to-coil efficiencies of the SS topology and the SN topology varying with the coupling coefficient under different quality factors are depicted in Fig. 6. With a large quality factor and a strong coupling, the difference in the maximum efficiency of the SS and SN topologies will not be significant. When the coupling coefficient is smaller than 0.5, the efficiency

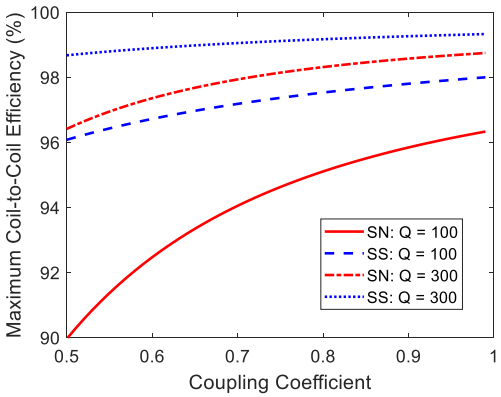

Fig. 6. Maximum coil-to-coil efficiency of the SS and SN topologies varying with coupling coefficient.

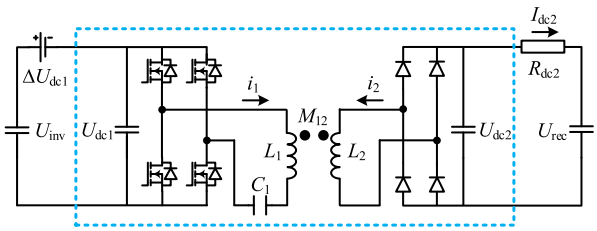

Fig. 7. Model of the SN topology in consideration of the voltage drops.

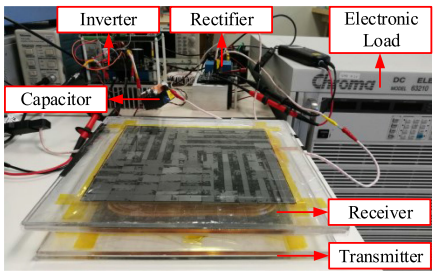

Fig. 8. Experimental prototype of the SN compensation.

difference between the SS topology and the SN topology would be significant. In this condition, employing the SN topology may not be a good choice. Therefore, the SN topology is a suitable solution to achieve a compact and low-cost receiver with a strong coupling and large coil quality factors.

C. Model in Consideration of Voltage Drops

In practical implementations, the output voltage of the SN topology may not always behave as shown in (23), because there are switch and coil losses and the voltages drops across the switches on both the transmitter and the receiver. The model of the SN topology in consideration of the losses and the voltage drops is given in Fig. 7, where ΔU_{dc1} is the voltage drop on the transmitter side and R_{dc2} is the total equivalent resistance (receiver resistance and rectifier resistance) on the receiver side. Inside the dash-line box is an ideal SN topology analyzed in Section III-B.

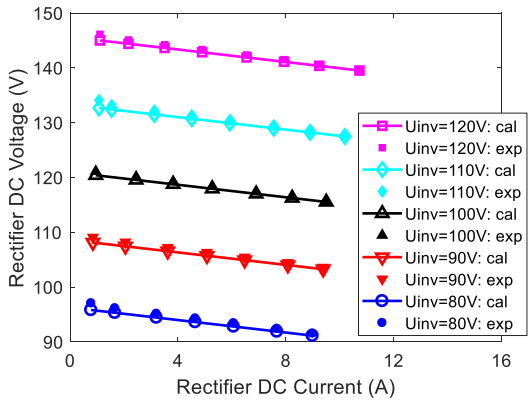

Fig. 9. Calculations and experimental results of U_{rec} varying with I_{dc2}.

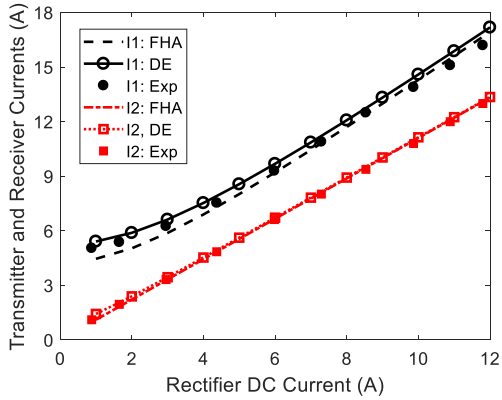

Fig. 10. Calculated and experimental results of transmitter and receiver currents varying with I_{dc2}.

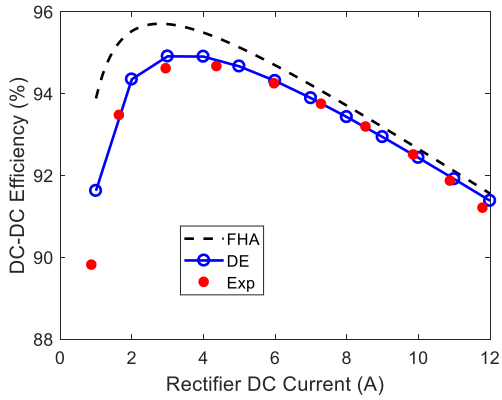

Fig. 11. Calculated and experimental results of dc–dc efficiency varying with I_{dc2}.

U_{dc2} and I_{dc2} can be expressed as

$$U_{dc2} = \frac{U_{bus} - \Delta U_{dc1}}{n} \tag{33}$$

$$I_{dc2} = \frac{U_{dc2} - U_{bat}}{R_{dc2}} = \left(\frac{U_{bus} - \Delta U_{dc1}}{n} - U_{bat}\right)\frac{1}{R_{dc2}}. \tag{34}$$

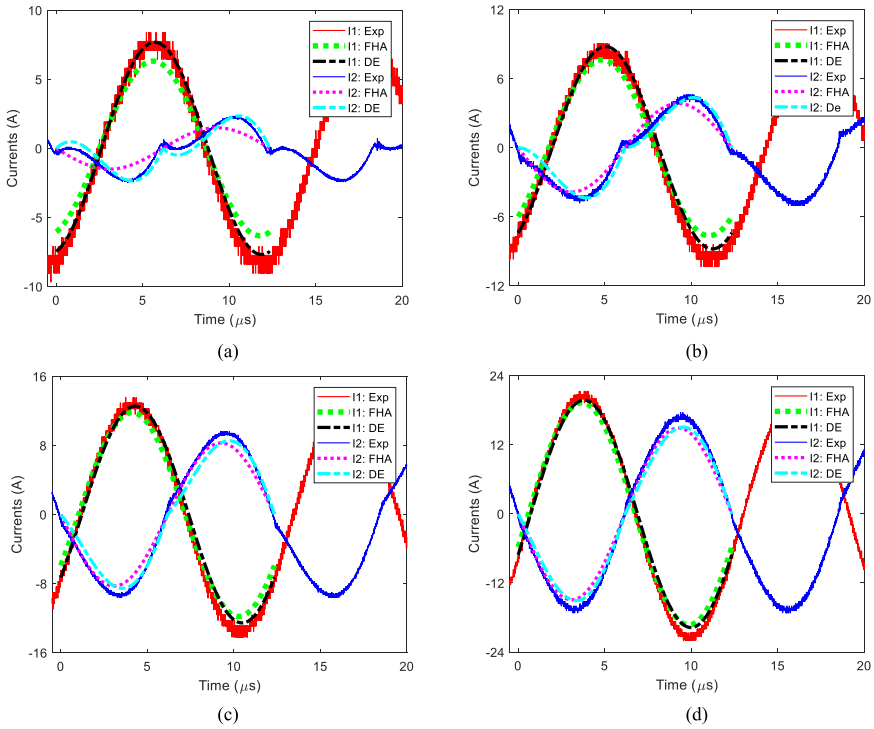

Fig. 12. Calculated and experimental waveforms of transmitter and receiver currents. (a) $I_{dc2} = 0.95$ A. (b) $I_{dc2} = 2.45$ A. (c) $I_{dc2} = 5.27$ A. (d) $I_{dc2} = 9.50$ A.

TABLE I
SYSTEM PARAMETERS OF SN TOPOLOGY

Note	Symbol	Value
Transmitter Inductance	L_1	63.5 μH
Receiver Inductance	L_2	61.9 μH
Mutual Inductance	M_{12}	49.9 μH
Coupling Coefficient	k_{12}	0.80
Leakage Inductance	L_r	23.25 μH
Transmitter Capacitance	C_1	166 nF
Main Inductance	L_m	40.2 μH
Turn Ratio	n	0.81
Resonant Frequency	f_r	81 kHz

IV. CALCULATIONS AND EXPERIMENTS

An experimental prototype of the SN topology is implemented to validate the analysis, as shown in Fig. 8. The system parameters are tabulated in Table I.

In this setup, ΔU_{dc1} is assumed to be 2 V and R_{dc2} is 0.57 Ω. The calculations and the experimental results of the rectifier dc voltage U_{rec} varying with the Rectifier dc current I_{dc2} under different dc voltages of the inverter U_{inv} are shown in Fig. 9. U_{rec} drops slowly with the increasing I_{dc2}, showing a voltage-source output characteristic.

When $U_{inv} = 100$ V, the calculated and experimental results of the transmitter and receiver currents and the dc–dc efficiency varying with the rectifier dc current are shown in Figs. 10 and 11, respectively. The calculated transmitter current based on FHA is smaller than that of DE, and because of this, the calculated efficiency based on FHA is larger than that based on DE. The model based on DE agrees better with the experimental results than that based on FHA. Therefore, for design the WPT system with the SN topology, the model based on DE is recommended.

When $U_{inv} = 100$ V, the calculated and experimental waveforms of the transmitter and receiver currents are shown in Fig. 12. FHA provides a good approximation when the output power is large. However, it is inaccurate when the power level is low. The calculated transmitter current based on FHA is always smaller than that based on DE, which is a verification of Fig. 10. In comparison, the proposed model based on DE agrees well with the experimental results at all power levels. The reason the receiver current is distorted at a low-power level is that the triangular component in the receiver current takes up a large proportion.

V. CONCLUSION

In this paper, an SN topology has been proposed for a WPT system with a strong coupling, featuring a compact structure of a noncompensated receiver and a lower receiver side loss. The SN topology achieves approximately the same efficiency as the SS topology when the coupling is strong and the coil quality factors are large. The SN topology is equivalent to the LLC converter and their correspondence has been investigated. The model of the SN topology has been built based on both FHA and DE. The model based on DE is more accurate than that based on

FHA, especially when the output power is small. The analytical expressions of the transmitter and receiver currents have been derived. It has been found that the transmitter current is purely sinusoidal, while the receiver current is distorted. The distorted receiver current has two components: the sinusoidal component and the triangular component. The triangular component is significant when the output power is small. The expression of the coil-to-coil efficiency has been derived and it is maximized at the phase difference between the transmitter voltage and current of $\pi/4$, or when the dc current of the rectifier equals the ratio of the dc voltage of the rectifier and the receiver reactance. An experimental prototype has been built. The proposed model well matches the experimental results in all power levels.

This paper is helpful for the optimal design of the SN topology in WPT systems with a strong coupling.

REFERENCES

[1] C. C. Mi, G. Buja, S. Y. Choi, and C. T. Rim, "Modern advances in wireless power transfer systems for roadway powered electric vehicles," *IEEE Trans. Ind. Electron.*, vol. 63, no. 10, pp. 6533–6545, Oct. 2016.

[2] B. H. Choi, E. Lee, Y. Sohn, G. Jang, and C. Rim, "Six degrees of freedom mobile inductive power transfer by crossed dipole Tx and Rx coils," *IEEE Trans. Power Electron.*, vol. 31, no. 4, pp. 3252–3272, Apr. 2016.

[3] Y. Zhang, Z. Zhao, and K. Chen, "Load matching analysis of magnetically-coupled resonant wireless power transfer," in *Proc. of IEEE ECCE Asia Downunder*, 2013, pp. 788–792.

[4] Z. Zhang, K. T. Chau, C. Qiu, and C. Liu, "Energy encryption for wireless power transfer," *IEEE Trans. Power Electron.*, vol. 30, no. 9, pp. 5237–5246, Sep. 2015.

[5] Z. Ye, Y. Sun, X. Dai, C. Tang, Z. Wang, and Y. Su, "Energy efficiency analysis of U-coil wireless power transfer system," *IEEE Trans. Power Electron.*, vol. 31, no. 7, pp. 4809–4817, Jul. 2016.

[6] C. Zhang, D. Lin, and S. Y. R. Hui, "Ball-joint wireless power transfer systems," *IEEE Trans. Power Electron.*, vol. 33, no. 1, pp. 65–72, Jan. 2018.

[7] R. Bosshard, J. W. Kolar, J. Muhlethaler, I. Stevanovic, B. Wunsch, and F. Canales, "Modeling and eta-alpha-Pareto optimization of inductive power transfer coils for electric vehicles," *IEEE J. Emerg. Sel. Topics Power Electron.*, vol. 3, no. 1, pp. 50–64, Mar. 2015.

[8] H. H. Wu, G. A. Covic, J. T. Boys, and A. P. Hu, "A 1kW inductive charging system using AC processing pickups," in *Proc. IEEE Conf. Ind. Electron. Appl.*, 2011, pp. 1999–2004.

[9] T. Kan, T. Nguyen, J. C. White, R. K. Malhan, and C. C. Mi, "A new integration method for an electric vehicle wireless charging system using LCC compensation topology: Analysis and design," *IEEE Trans. Power Electron.*, vol. 32, no. 2, pp. 1638–1650, Feb. 2017.

[10] L. Zhao, D. J. Thrimawithana, and U. K. Madawala, "Hybrid bidirectional wireless EV charging system tolerant to pad misalignment," *IEEE Trans. Ind. Electron.*, vol. 64, no. 9, pp. 7079–7086, Sep. 2017.

[11] A. Foote and O. C. Onar, "A review of high-power wireless power transfer," in *Proc. IEEE Transp. Electrification Conf. Expo*, 2017, pp. 234–240.

[12] F. Jolani, Y. Yu, and Z. Chen, "Enhanced planar wireless power transfer using strongly coupled magnetic resonance," *Electron. Lett.*, vol. 51, no. 2, pp. 173–174, Jan. 2015.

[13] C. Kim, D. Seo, J. You, J. Park, and B. H. Cho, "Design of a contactless battery charger for cellular phone," *IEEE Trans. Ind. Electron.*, vol. 48, no. 6, pp. 1238–1247, Dec. 2001.

[14] B. Choi, J. Nho, H. Cha, T. Ahn, and S. Choi, "Design and implementation of low-profile contactless battery charger using planar printed circuit board windings as energy transfer device," *IEEE Trans. Ind. Electron.*, vol. 51, no. 1, pp. 140–147, Feb. 2004.

[15] J. Deng, S. Li, S. Hu, C. C. Mi, and R. Ma, "Design methodology of LLC resonant converters for electric vehicle battery chargers," *IEEE Trans. Veh. Technol.*, vol. 63, no. 4, pp. 1581–1592, May 2014.

[16] Y. Zhang, Z. Zhao, and K. Chen, "Frequency decrease analysis of resonant wireless power transfer," *IEEE Trans. Power Electron.*, vol. 29, no. 3, pp. 1058–1063, Mar. 2014.

Yiming Zhang (S'13–M'16) received the B.S. and Ph.D. degrees in electrical engineering from Tsinghua University, Beijing, China, in 2011 and 2016, respectively.

He is currently a Post-Doctoral Researcher with the San Diego State University, San Diego, CA, USA. His research interests include wireless power transfer for electric vehicles and mobile phones, and resonant converters.

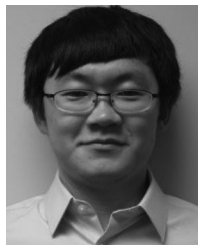

Tianze Kan (S'15) received the B.Eng. degree in electrical engineering and automation from Huazhong University of Science and Technology, Wuhan, China, in 2011 and the M.S. degree in electrical engineering from the University of Southern California, Los Angeles, CA, USA, in 2013. He is currently working toward the Ph.D. degree in electrical and computer engineering in the joint doctoral program between San Diego State University, San Diego, CA, USA, and the University of California San Diego, La Jolla, CA.

His research interests include power electronics and inductive-based wireless power transfer, especially on coil design and compensation topologies.

Zhengchao Yan (S'18) received the B.S. degree in mechanical design, manufacturing and automation from Northwestern Polytechnical University, Xi'an, China, in 2013, where he is currently working toward the Ph.D. degree. In 2017, he received the funding from China Scholarship Council, and became a joint Ph.D. student with the Department of Electrical and Computer Engineering, San Diego State University, San Diego, CA, USA.

His research interests include wireless power transfer, including coil design and compensation topologies.

Yunhe Mao received the Master's degree from the Harbin Institute of Technology, Shenzhen, China, in 2010.

He is currently a Senior Researcher with the CRI of Huawei Technologies Co., Ltd., Shenzhen, China. From 2010 to 2015, he was with the EMERSON network power China for UPS product development. His research interests include wireless power transfer for electric vehicles, UPS topologies, and control method.

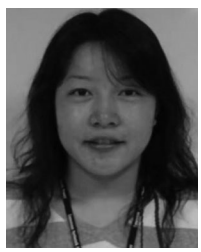

Zhixian Wu received the Master's degree from the South China University of Technology, Guangzhou, China, in 2005.

She is currently a Senior Researcher with the CRI of Huawei Technologies Co., Ltd., Shenzhen, China. From 2005 to 2015, she was with the EMERSON network power China for advanced power electronic technology research. Her research interests include wireless power transfer for electric vehicles, converter topologies, and WBG switches.

Chunting Chris Mi (S'00–A'01–M'01–SM'03–F'12) received the B.S.E.E. and M.S.E.E. degrees in electrical engineering from Northwestern Polytechnical University, Xi'an, China, in 1985 and 1988, respectively, and the Ph.D. degree in electrical engineering from the University of Toronto, Toronto, ON, Canada, in 2001.

He is currently a Professor, the Chair of electrical and computer engineering, and the Director of the Department of Energy–funded Graduate Automotive Technology Education Center for Electric Drive Transportation, San Diego State University, San Diego, CA, USA. Prior to joining San Diego State University, he was with the University of Michigan, Dearborn from 2001 to 2015. His research interests include electric drives, power electronics, electric machines, renewable-energy systems, and electric and hybrid vehicles.